



LAWRENCE  
LIVERMORE  
NATIONAL  
LABORATORY

# A Methodology for the Indirect Determination and Spatial Resolution of Shear Modulus of PDMS-Silica Elastomers

B. Mayer, J. Reimer, R. Maxwell

September 4, 2007

Chemical Engineering Science

This document was prepared as an account of work sponsored by an agency of the United States Government. Neither the United States Government nor the University of California nor any of their employees, makes any warranty, express or implied, or assumes any legal liability or responsibility for the accuracy, completeness, or usefulness of any information, apparatus, product, or process disclosed, or represents that its use would not infringe privately owned rights. Reference herein to any specific commercial product, process, or service by trade name, trademark, manufacturer, or otherwise, does not necessarily constitute or imply its endorsement, recommendation, or favoring by the United States Government or the University of California. The views and opinions of authors expressed herein do not necessarily state or reflect those of the United States Government or the University of California, and shall not be used for advertising or product endorsement purposes.

# A Methodology for the Indirect Determination and Spatial Resolution of Shear Modulus of PDMS-Silica Elastomers

Brian P. Mayer\*, Jeffrey A. Reimer†, Robert S. Maxwell‡

August 29, 2007

A methodology is described that allows for the spatial resolution of shear modulus in silica-filled PDMS elastomers via  $^1\text{H}$  relaxation measurements and stray-field imaging (STRAFI) techniques. Traditional Hahn echoes provide a simple, robust route to the extraction of a proton residual dipolar coupling constant (RDC), a direct measure of chain mobility and a parameter that can be correlated to numerous mechanical properties. Defining a dimensionless RDC eliminates any artifacts associated with low-field measurement and allows the RDC to become independent of field strength. A direct correlation between the NMR determined dimensionless RDC and results from dynamic mechanical analysis is presented, then employed via STRAFI to determine spatial variations in moduli associated with irradiated elastomeric materials. Reliable performance, despite poorly optimized STRAFI conditions, is demonstrated with an error of no more than 22% between the calculated shear modulus and the measured value via DMA.

---

\*Department of Chemical Engineering, University of California, Berkeley, 94720

†Department of Chemical Engineering, University of California, Berkeley, 94720

‡Lawrence Livermore National Laboratory, Livermore, California, 94551

# 1 Introduction

There is considerable need for the development and practical application of methods that can elucidate structural and dynamical changes associated with polymer degradation and aging. For example, the demanding environments to which poly(dimethylsiloxane)-based (PDMS-based) elastomeric materials are exposed often induce subtle microscopic changes of engineering concern resulting in limited device lifetimes. Broadly speaking, experimental methods for the characterization of polymer degradation must be sensitive to changes that occur upon exposure to harsh chemical, physical, mechanical and radiological environments. Most desirable would be a technique that provides spatial resolution in a non-invasive and non-destructive fashion, yet remains a relatively simple analytical methodology.

Nuclear magnetic resonance spectroscopy (NMR) has been employed for the fundamental studies of polymer-containing materials for over thirty years. Data from these studies show strong correlations between several NMR observables and polymer mechanical properties.[1][2][3][4][5] In the case of elastomeric materials, these properties are dictated to a large degree by network topology. The motional restrictions imposed by chemical crosslinks and physical entanglements prevent complete (i.e. isotropic) chain reorientation on the NMR timescale thus partially preserving spatially dependent interactions, in particular the nuclear magnetic dipolar interaction.

More recently, magnetic resonance imaging methods have been employed to provide spatial resolution of residual dipolar interactions through measurement of, for example, transverse ( $T_2$ ) magnetization decay and multiple quantum coherence buildup.[6][7] In this fashion one can ostensibly map out not only spin density on a pixel-by-pixel basis but also measures of molecular mobility on the order of  $< 1mm$  in soft materials.

In this paper we seek to demonstrate the application of residual dipolar couplings (RDCs)

towards the imaging of mechanical properties in radiation-damaged silica-filled PDMS elastomers. We determine these couplings for elastomers subjected to various exposures of gamma-radiation, correlate them to moduli obtained from dynamic mechanical analysis, and show that moduli can then be imaged using simple MRI methodologies. The correlation between RDC and modulus is scalable down to magnetic fields typically used in portable MR devices, portending the development of standoff *ex-situ* assessment of elastomeric moduli.

## 2 Experimental

The samples studied were a series of poly(dimethylsiloxane)-poly(diphenylsiloxane) silica-filled elastomers exposed to 5 cumulative doses of up to 50 MRad of  $\gamma$ -irradiation. The pristine sample, unexposed to radiation, was also studied. The details of their preparation and composition can be found elsewhere.[?]

$^1\text{H}$  NMR was conducted at magnetic fields of 0.49, 1.54, and 4.70 Tesla at room temperature under static conditions. The mid-field data were taken with a LapNMR spectrometer (Tecmag, Houston, TX) operating at 65.614 MHz. The low-field data were obtained on a permanent magnet also with a LapNMR spectrometer at 20.7 MHz. Due to the magnet's temperature sensitivity (field shift of approximately 5 kHz/ $^{\circ}\text{C}$ ) an environmental controller was built to house the magnet and keep the temperature constant within 0.2 $^{\circ}\text{C}$ . High-field work was done on an AMX200 spectrometer (Bruker, Billerica, MA) at 200.13 MHz. All experiments were performed at 25 $^{\circ}\text{C}$  under static conditions, as the highly mobile networks provided significantly narrower proton line-widths than those typically seen with polymeric materials, which often exceed 10 kHz. Additionally, as room temperature is significantly above the polymer's glass transition temperature ( $T > T_g + 50^{\circ}\text{C}$ ), chain mobility will be not dominated by thermal motion but instead only by the topological constraints

restricting it (i.e., chemical and physical crosslinks and entanglements).

Transverse magnetization decay curves were obtained using the standard Hahn echo,  $(\pi/2)_x - \tau - (\pi)_y - acquire$ , combined with CYCLOPS to remove instrumental artifacts. Data were obtained using both commercial and home-built probes, but the  $\pi/2$  pulse length was kept around  $1.5 \mu\text{sec}$  for all experiments. Due to  $^1\text{H}$  natural abundance and the probes' relatively high Q values, in general only 12-24 scans were required for exceptional signal-to-noise for a  $1\text{-}2 \text{ mm}^3$  sample volume. A typical experiment was on the order of 3 hours given a repetition delay of 4 seconds.

Images of the samples were acquiring using stray-field imaging techniques[9] (STRAFI) at 299.32 MHz with an Apollo console (Tecmag, Houston, TX). The resultant images were one-dimensional and obtained in a constant magnetic field gradient of 0.2 G/cm with little optimization. The strength of the gradient was measured by both glycerol and water diffusion experiments and confirmed by imaging a sample of known length. This relatively low gradient strength was chosen to maintain high signal-to-noise per pixel, as well as demonstrate the technique's validity despite very little additional experimental optimization. The  $\pi/2$  pulse length of  $10 \mu\text{sec}$  was chosen to ensure relatively uniform excitation across the entire sample height. Spectra were obtained using the Hahn echo method described above. 100 spectra were taken all together which contained each 512 signal averages. With a repetition delay of 4 seconds, this experiment was 2.5 days in duration.

For all three field strengths used in the relaxation studies, data were analyzed by integrating under the magnitude of the FID and baseline correcting in post-processing. This procedure accounted for any small field drifts of the permanent magnet. Extracted decay curves were normalized to the magnetization after a one-pulse experiment and equivalent experimental conditions (e.g. number of scans, receiver gain, etc.) and fit using nonlinear regression techniques in a standard computational mathematics package. STRAFI images were analyzed in an identical fashion, though the

real component of the Fourier transformed, phased spectra was used.

## 3 Results and Discussion

### 3.1 Measurement of proton residual dipolar coupling.

As mentioned above, determination of the residual dipolar coupling for this work was done via  $T_2$  decay curves. This method was chosen by virtue of both its experimental and analytical simplicity. Recently, other techniques have been shown to be more accurate, as spin-echo experiments can obfuscate RDC measurement as a result of, for example, dubious model assumptions and fitting ambiguities.[10][11] In general, this group has found at most a 15% difference in the couplings measured via  $T_2$  decay and a sine-correlation experiment[12] which filters out all signal but that of dipolar origin (unpublished data). Moreover, since we are presently only concerned with *relative* changes in the RDC magnitude, we feel that the spin-echo method is adequate.

Figure 1 shows representative transverse magnetization decays for the pristine, 1 and 50 MRad samples at 65 MHz. The solid- and liquid-like decays (due to motionally-hindered protons and completely mobile protons, respectively) are temporally separated by virtue of the frequencies of their motions in relation to each other. Proton pairs contained within liquid-like components are able to sample the entire solid angle, effectively averaging out the dipolar interaction, whereas those of solid-like components only experience a partial averaging of this interaction over the time-scale of the NMR experiment.

Even though the short-term signal decay determines the RDC magnitude, we have chosen to fit the entire decay envelope since the signal to noise ratio is so high ( $\approx 100$  at short delay times); additionally we were able to obtain the relative contributions to the total decay curve. The data have

been fit to an expression for the decay of transverse magnetization,  $M_x$ , assuming its applicability to polymer chains subject to topological constraints.  $M_x(\tau)$ , as a function of echo time,  $\tau$ , is given by the normalized equation

$$\frac{M_x(\tau)}{M_x(0)} = x_1 \exp \left[ -M_2 \tau^2 \right] + \sum_{i=2}^4 x_i \exp \left[ -\frac{\tau}{T_{2,i}} \right] \quad \text{with } \sum_{i=1}^4 x_i = 1 \quad (1)$$

where  $x_1$  is the relative amount of protons described by  $M_2$ , the residual second moment of the dipolar line-width; and  $x_i$  represent one of three transverse relaxation times,  $T_{2,i}$ . Note the longest  $T_2$  value corresponds to a small fraction ( $< 5\%$ ) of protons associated with freely mobile dangling chain ends,  $T_2^{de}$ .  $T_2^{de}$  has been fixed at 32.5 msec based on measurements of the unfilled, uncrosslinked gum stock.

Under the Anderson-Weiss formalism,  $M_2$  ( $\text{msec}^{-2}$ ) is related to the residual dipolar coupling constant,  $D_{res}$  (Hz) by the van Vleck second moment:

$$M_2 = \frac{9}{20} \left( \frac{2\pi \cdot D_{res}}{1000} \right)^2. \quad (2)$$

Despite identifying several protons environments with different relaxation parameters in accordance with Equation 1, reported in the first two columns of Table 1 is solely  $D_{res}$  as a function of radiation dose taken at 65 MHz and 200 MHz.

At these two fields, the RDC in general increases over the dosage range, pointing toward reduced motional averaging of the dipolar interaction due to radiation-induced crosslinking of side chains. In contrast, an interesting phenomenon appears at low dosage levels at which a decrease in RDC is observed, implying an increase in segmental mobility. Recent studies have explained this observation in terms of hydrogen bond interruption and a concomitant release of chains at the silica-polymer interface.[8]

In effort to demonstrate the applicability of this technique at low field, the same data were

acquired on a 20 MHz permanent magnet. Previous reports have demonstrated the difficulty in acquiring reliable estimates of RDCs at low fields where field inhomogeneities and susceptibility effects from filler particles can play a large role in clouding their measurement.[13] Nevertheless, we have attempted to obtain estimates of the RDCs for the pristine and five irradiated samples. Note that the reliability of these measurements depend heavily on not only the model chosen to represent the transverse magnetization decay but also on the quality of the decay data obtained, particularly when the proton component associated with the residual second moment is comparatively small.

The last column of Table 1 shows the 20MHz RDC measured for the samples as compared to the data taken at high field. While a low signal to noise ratio (SNR) is not unexpected at 20 MHz, since it scales with the magnetic field strength, the relatively poor SNR seen here precipitated overestimation of the RDCs by about 50% when compared to data at 65 and 200 MHz. As shown in Figure 2, however, comparison of the initial decay curves out to 1.5 msec (where the component associated with the RDC dominates) shows identical decay patterns suggesting that SNR is affecting RDC extraction to the largest degree as opposed to systematic low-field effects such as microscopic magnetic field gradients at the filler interface.

To compensate for this overestimation, a new variable can be created that represents the relative change in RDC as a function of dosage; or in other terms, one that references the RDC at a given dosage,  $D_{res}^d$ , to that of the pristine sample,  $D_{res}^0$ . This quantity,  $D^*$ , can be expressed as

$$D^* \equiv \frac{D_{res}^d - D_{res}^0}{D_{res}^0} \quad (3)$$

whereby, for example, a negative value indicates softening in comparison to the pristine sample. Table 2 and Figure 3 both show this reduced RDC for all dosages and field strengths. For all fields investigated,  $D^*$  is relatively constant for a given radiation dose implying that correlating it to a particular mechanical property is advantageous over its absolute counterpart, as this normalization

scheme effectively removes any possible low-field artifacts.

### 3.2 Establishing an NMR/shear modulus correlation.

To establish a theoretical link between proton residual dipolar coupling and a macroscopic structural parameter such as shear modulus, we seek to establish a common dependency. The RDC between two protons located on a polymer chain subject to Gaussian statistics can be expressed as[14]

$$D_{res,jk} = \frac{3}{5} \frac{\mathbf{R}^2}{N^2 a^2} b_{jk} P_2(\cos \chi) \quad (4)$$

where  $\mathbf{R}$  is the end-to-end vector of a chain between two crosslinks,  $N$  is the number of statistical segments of length  $a$ ,  $b_{jk}$  is the rigid dipolar coupling constant, and  $P_2(\cos \chi)$  is the second order Legendre polynomial with respect to the angle between the end-to-end vector and the external magnetic field. Approximating the polymer network as one of Gaussian disordered chains, a dimensionless end-to-end vector can be defined which is on the order of unity,

$$\mathbf{q}^2 = \frac{\mathbf{R}^2}{\langle \mathbf{R}^2 \rangle_{\mathbf{R}}} = \frac{\mathbf{R}^2}{Na^2} \approx 1 \quad (5)$$

such that the RDC scales merely as the inverse of the number of chain units,  $N^{-1}$ . The storage modulus,  $G'$  also scales with the inverse of  $N$  through a direct dependence on the crosslink density,  $v_c$ , [15]

$$G' = v_c k_b T \propto N^{-1}. \quad (6)$$

Therefore, assuming the Gaussian assumption holds, there should be a proportional relationship between the residual dipolar coupling and shear modulus.

Table 3 shows shear modulus data for these samples adapted from Maxwell, et al.[8] Figure 4a shows the combination of these data with RDC measurements at both 200 MHz and 65 MHz. Since, however, the absolute RDC data is dependent on the field at which they are measured, we

have chosen to establish the modulus/NMR correlation using the normalized  $D^*$  scheme. Linear regression for these data yield

$$G' = 117[\text{GPa}]D^* + 238[\text{GPa}]. \quad (7)$$

The intercept at 238 GPa represents the fit at  $D^* = 0$  and an estimation of shear modulus in the absence of irradiation. This corresponds well, within 5%, of the measured value (see Table 3). The relatively high slope of 117 GPa indicates there will be high sensitivity to shear modulus variations for even small changes in the reduced RDC. This fact also requires, however, careful measurement of the residual dipolar coupling constant.

Employing Equation 7 there now exists the ability to indirectly determine the modulus, a macroscopic quantity, simply by measuring an NMR parameter that is dictated primarily by polymer chain mobility. An even more useful result, perhaps, is that this correlation is independent of the mechanisms affecting network structure. The data displayed in both graphs of Figure 4 represent the entire irradiation range including both the softening effect that dominates at low dosages and the high-dosage crosslinking. In particular the  $D^*/G'$  correlation, has shown to be robust to *both* the magnetic field and various degradation mechanisms.

### 3.3 Application of the $D^*/G'$ correlation.

For the present work, a sandwich of three samples of different dosages each were made and placed in a 10mm NMR tube (see Figure 5), and one-dimensional images were obtained to test the accuracy of the above correlations in tandem with the imaging modality. The sandwich was constructed to contain modest  $G'$  contrast between layers. The direction of the stray field gradient was assumed to be normal to the broad face of the individual sandwich components, but it is important to note that no detailed field mapping was done to determine gradient variation across the sample or any

nonlinearities that, of course, in reality, are present.

Figure 6 shows a summary of the STRAFI data. Extraction of the residual second moment,  $M_2$ , was fairly straightforward, with values comparable to those of the bulk relaxation measurements. The values are larger overall, which is merely an effect of the magnetic field inhomogeneities artificially increasing relaxation rates. Employing the methodology outlined above, we convert  $M_2$  to  $D_{res}$  and  $D_{res}$  to  $D^*$  via Equations 2 and 3, respectively. Use of Equation 7 yields the calculated  $G'$  values shown in the figure. As indicated in the caption the bold line represents the modulus as measured by DMA. The lack of a clear break in the  $M_2$  and calculated  $G'$  values at the sample interfaces (pixels 1006 and 1023) results from the low gradient strength, as the frequency spread for a given pixel barely overcomes the natural proton linewidth. This fact explains the apparent continuum of values seen across the sandwich height; there is, in effect, a *bleed-through* of information between pixels. Moreover, there is no need to know the gradient strength or nonlinearities across the sample, as the correlation does not require this type of information. Despite these potentially serious pitfalls, the error between the correlated and measured (i.e. NMR vs. DMA) values is at most 20% which is quite good considering this lack of optimization usually present in STRAFI experiments.

As this methodology is clearly independent of the imaging modality, one could quite easily extend it to multiple dimensions, acquiring a fully three-dimensional data set. Using pulsed field-gradient imaging techniques would certainly only enhance the data quality, as the experimentalist would have full control over gradient strength and linearity and would be able to suppress artifacts due to natural linewidth bleed-through. One minor complication, that being the acquisition of images at short delay times, could be easily compensated for by the use of SPRITE techniques developed to address just this issue.[16]

## 4 Conclusions

The present work has demonstrated the utility of transverse magnetization decay in the extraction of proton residual dipolar coupling constants and their subsequent imaging. Despite recent criticism of various  $T_2$  methods, we have demonstrated the present methodology to be more than adequate since we are presently only concerned with relative changes in the RDC magnitude, as opposed to their absolute counterparts. These data were used in conjunction with dynamic mechanic analysis to establish a correlation between a measure of chain mobility and the bulk shear modulus of PDMS-silica elastomers. A field-independent, reduced RDC was defined that opened up the possibility of low-field measurement, making this technique particularly attractive, as inexpensive permanent magnets and portable single-sided systems are more amenable to efficient, in-field diagnostics.

## References

- [1] Marcinko, J. J.; Parker, A. A.; Shieh, Y. T.; Ritchey, W. M. *J. Appl. Polym. Sci.* **1992**, *45*, 391-398.
- [2] Parker, A. A.; Marcinko, J. J.; Rinaldi, P.; Hedrick, D. P.; Ritchey, W. M. *J. Appl. Polym. Sci.* **1993**, *48*, 677-681.
- [3] Fischer, E.; Grinberg, F.; Kimmich, R.; Hafner, S. *J. Chem. Phys.* **1998**, *109*, 846-854.
- [4] Litvinov, V. M.; Dias, A. A. *Macromolecules* **2001**, *34*, 4051-4060.
- [5] Fechete, R.; Demco, D. E.; Blümich, B. *J. Chem. Phys.* **2003**, *118*, 2411-2421.
- [6] Klinkenberg, M.; Blümmler, P.; Blümich, B. *Macromolecules* **1997**, *30*, 1038-1043.
- [7] Fechete, R.; Demco, D. E.; Blümich, B. *J. Mag. Res.* **2003**, *165*, 9-17.

- [8] Maxwell, R. S.; Balazs, B. *J. Chem. Phys.* **2002**, *116*, 10492-10502.
- [9] McDonald, P. J.; Newling, B. *Rep. Prog. Phys.* **1998**, *61*, 1441-1493.
- [10] Whittaker, A. K.; Bremner, T.; Zelaya, F. O. *Polymer* **1995**, *36*, 2159-2164.
- [11] Saalwächter, K. *Prog. Nucl. Magn. Reson. Spectrosc.* **2007**, *51*, 1-35.
- [12] Callaghan, P. T.; Samulski, E. T. *Macromolecules* **1997**, *30*, 113-122.
- [13] Saalwächter, K. *Macromolecules* **2005**, *38*, 1508-1512.
- [14] Sotta, P.; Deloche, B. *Macromolecules* **1990**, *23*, 1999-2007.
- [15] Jenkins, R. K. *J. Polym. Sci.* **1966**, *4*, 41-52.
- [16] Kennedy, C. B.; Balcom, B. J.; Kastikhin, I. V. *Can. J. Chem.* **1998**, *76*, 1753-1765.

## 5 Figures and Charts

These begin on the subsequent page.

This work performed under the auspices of the U.S. Department of Energy by Lawrence Livermore National Laboratory under Contract DE-AC52-07NA27344.

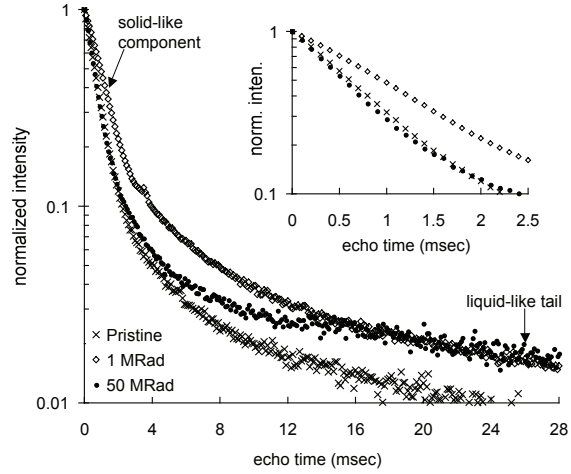


Figure 1:  $T_2$  decay curves for pristine ( $\times$ ), 1 MRad ( $\diamond$ ), and 50 MRad ( $\bullet$ ), samples at 65 MHz. The solid-like decay dominates at short echo times whereas liquid-like populations are seen at times greater than approximately 16 msec. The inset shows the short time decay which is dictated by the motionally-hindered, dipolar-coupled protons.

Table 1:  $D_{res}$  as a function of radiation dosage at 65, 200, and 20 MHz.

Dose (MRad)	$D_{res}$ (Hz) at 65 MHz	$D_{res}$ (Hz) at 200 MHz	$D_{res}$ (Hz) at 20 MHz
0	$260 \pm 10$	$231 \pm 10$	$383 \pm 23$
1	$166 \pm 8$	$159 \pm 8$	$275 \pm 18$
5	$176 \pm 4$	$168 \pm 10$	$260 \pm 13$
10	$178 \pm 4$	$196 \pm 15$	$302 \pm 20$
25	$230 \pm 3$	$225 \pm 12$	$367 \pm 19$
50	$336 \pm 3$	$317 \pm 16$	$519 \pm 21$

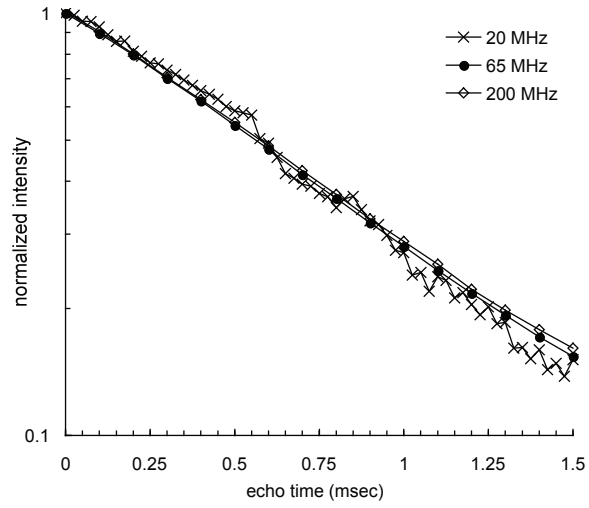


Figure 2: Comparison of initial transverse decay for pristine sample at 20 MHz ( $\times$ ), 65 MHz ( $\bullet$ ), and 200 MHz ( $\diamond$ ). Discussion of graph found in text.

Table 2:  $D^*$  as a function of radiation dosage at all three fields. Error is estimated at no more than 15%.

Dose (MRad)	$D^*$ at 20 MHz	$D^*$ at 65 MHz	$D^*$ at 200 MHz
1	-0.28	-0.38	-0.28
5	-0.32	-0.35	-0.25
10	-0.22	-0.30	-0.14
25	-0.04	-0.09	-0.02
50	0.36	0.32	0.34

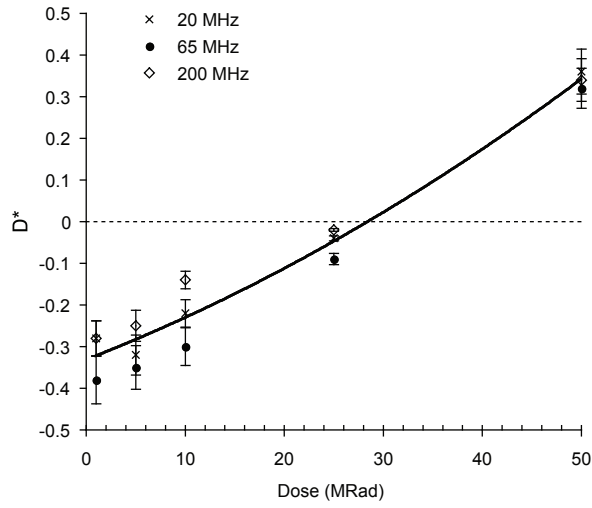


Figure 3: The field-independence of the reduced RDC,  $D^*$ , as a function of dosage at 20 MHz ( $\times$ ), 65 MHz ( $\bullet$ ), and 200 MHz ( $\diamond$ ). The bold line is merely a guide for the eye, and the dashed line demarcates the transition from softened to stiffened as compared to the pristine sample.

Table 3: Dynamic Mechanical Analysis:  $G'$  as a function of dosage.[8]

Dose (MRad)	$G'$ (GPa)
0	227.0
1	216.6
5	192.2
10	215.8
25	229.0
50	284.5

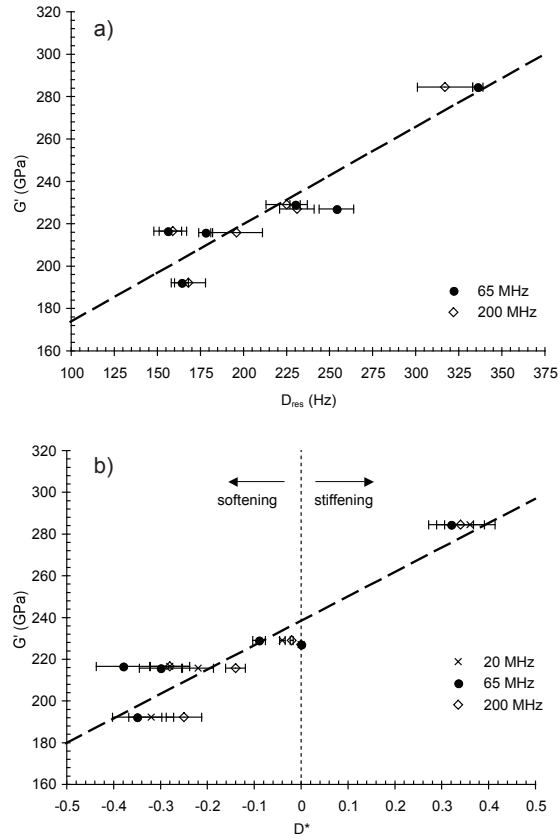


Figure 4: a) Relation of  $G'$  to  $D_{res}$  at 65 (●) and 200 MHz (◇). b)  $G'$  versus  $D^*$  at all three fields: 20 (×), 65 (●) and 200 MHz (◇). The thick dashed line is the fit according to Equation 7. The thin vertical dashed line represents  $D^* = 0$ , and the arrows indicate the dominant degradation pathway relative to the pristine sample.  $R^2 \approx 0.89$ .

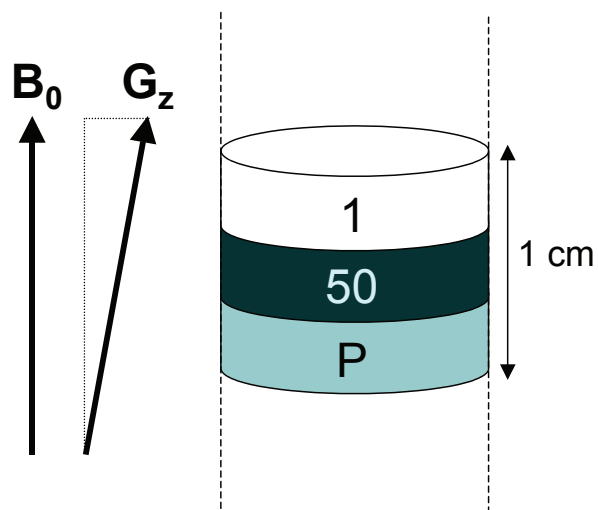


Figure 5: Pictorial representation of elastomer sandwich. Application of the magnetic field gradient,  $G_z$  was assumed to be co-linear with the static magnetic field,  $B_0$  as shown in the diagram. Relative moduli values have been cartooned by shading the slices in various gray tones. Dashed lines indicate 10mm quartz NMR tube.

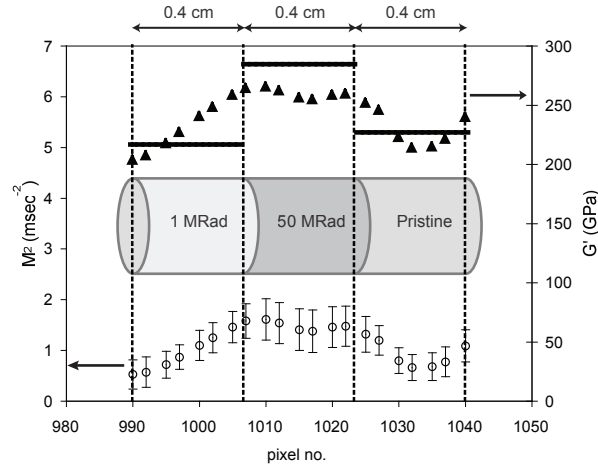


Figure 6: The spatial resolution of residual second moment,  $M_2$ , and shear modulus,  $G'$ . Open circles are pixel-by-pixel  $M_2$  values extracted from the STRAFI data. Filled triangles are  $G'$  calculated from Equation 7, and for comparison, the bold lines represent the modulus measured via DMA. The sample sandwich has been underlaid for clarity, and the dashed vertical lines indicate boundaries of the individual sandwich components. Sample size has also been indicated above the graph. Total height of sample is 1.2 cm.